Design Rules for Slanted-Angle Polarization Rotators

Henghua Deng, *Member, OSA*, David O. Yevick, *Fellow, IEEE, Fellow, OSA*, Chris Brooks, and Paul E. Jessop, *Member, IEEE*

***Abstract*—A simple and general set of design rules for slanted-angle polarization-rotating waveguides is presented in this paper. These design rules are employed to construct single-mode SOI polarization rotators that offer significant advantages in conversion efficiency, optical loss, fabrication tolerance, spectral response and spatial dimensions relative to III–V components.**

***Index Terms*—Dense-wavelength-division multiplexing (DWDM), finite-element method (FEM), integrated optics, optical waveguide, planar lightwave circuit (PLC), polarization rotator, silicon-on-insulator (SOI), single-mode condition, III–V semiconductor.**

I. Introduction

As optical fiber systems evolve to higher data rates, the importance of polarization control and manipulation steadily increases. Passive polarization rotators are central to such systems and are generally composed of concatenated segments, each of which rotates the light polarization a small amount, or a single, long slanted-angle waveguide. InGaAsP longitudinally periodic [1]–[3] and bent structures [4] were the first structures realized, followed by single-section slanted-angle polarization rotators fabricated in both GaAs and InP [5]–[7].

Compared with III–V waveguides of equivalent dimensions, silicon-on-insulator (SOI) waveguides provide stronger optical confinement [8]. Further, single-mode yet large cross-section SOI waveguides (with, e.g., a silicon film thickness of 3–10 μm) can be fabricated at relatively low cost. As a result, both the coupling loss to single-mode fibers and the fabrication tolerance are enhanced. In this paper, the design of slanted-angle SOI polarization rotators is considered accordingly. In addition, SOI and III–V converters are compared and general design procedures are proposed.

In slanted-angle waveguides, the modes are hybridized by the geometric asymmetry, becoming transverse electric (TE) and transverse magnetic (TM) with respect to the slanted facet rather than the substrate interface. In multiple-section polarization rotators, the modes are typically weakly hybridized, while modes in single section devices are fully hybridized with nearly equal TE and TM components in each of the two orthogonal fundamental modes. In the latter case, the optical axis is positioned at a 45° with respect to the lateral direction while the intensities of the two fundamental modes will be comparable. The polarization of an incoming TE or TM mode is therefore rotated by 90° after a half-beat length

$$L_\pi = \frac{\pi}{\beta_1 - \beta_2} \tag{1}$$

where β_1 and β_2 are the propagation constants of the two fundamental modes.

Numerous simulations of III–V polarization rotators have been performed using the finite-difference method (FDM) [6], [7], [9], [10]; the finite-element-method (FEM) mode solver [2], [5], [11], [12]; the finite-element beam-propagation method (FE-BPM) [13]; the finite-element-based genetic algorithm [14]; and the vectorial boundary-element method (V-BEM) [15].

In this paper, these analyses are extended by developing a systematic design procedure that can be applied to general waveguide profiles and material systems. The maximum polarization rotation, single-mode condition, and modal coupling lengths are first graphed as a function of various waveguide parameters. From this information, a simple empirical formula is derived which can be employed to design SOI converters over a wide range of silicon film thicknesses and to predict fabrication tolerances.

II. Waveguide Geometry

The geometry of a general passive slanted-angle polarization rotator is displayed in Fig. 1(a). Standard III–V devices are based on either the symmetric external layer structure of Fig. 1(b), [2], [5], [6], [11]–[14] or that of Fig. 1(e), [7], [9], [10]. In this paper, however, we focus on the asymmetric external layer structure of Fig. 1(c).

In the figure, H denotes the total rib height, which in the case of SOI waveguides is identical to the thickness of the silicon guiding film, so that a 3-μm SOI design in this paper refers to $H = 3$ μm. Further, W is the width at the base of the rib, and θ is the angle formed by the slanted-angle facet that to simplify fabrication generally coincides with a crystal plane, e.g., $\theta = 54.736°$ for the (111) plane in Si and $\theta \approx 52°$ for InGaAsP. The symbols h, h_r, d_c, d_p, d_i, and d_s denote the thicknesses of the external layer adjacent to the vertical rib facet, the external layer adjacent to the slanted facet, the region between the top of the rib and the end of the computational window, the cap, the insulator, and the substrate layers, respectively. The computational window dimensions are X_{sl} and X_{sr}. In the figure, as in the rest of the paper ,we define the ratio of the slab thickness to

Manuscript received September 5, 2003; revised April 28, 2004. This work is supported in part by Nortel Networks, by the Canadian Institute for Photonic Innovations (CIPI), and by the Natural Science and Engineering Research Council of Canada (NSERC).

H. Deng is with the Department of Electrical and Computer Engineering, University of Waterloo, Waterloo, ON N2L 3G1, Canada (e-mail: hdeng@uwaterloo.ca).

D. O. Yevick is with the Department of Physics and the Department of Electrical and Computer Engineering, University of Waterloo, Waterloo, ON N2L 3G1, Canada (e-mail: yevick@uwaterloo.ca).

C. Brooks and P. E. Jessop are with the Centre for Electrophotonic Materials and Devices, Department of Engineering Physics, McMaster University, Hamilton, ON L8S 4L7, Canada (e-mail: brookscj@mcmaster.ca; pjessop@mcmaster.ca).

Digital Object Identifier 10.1109/JLT.2004.834477

0733-8724/$20.00 © 2005 IEEE

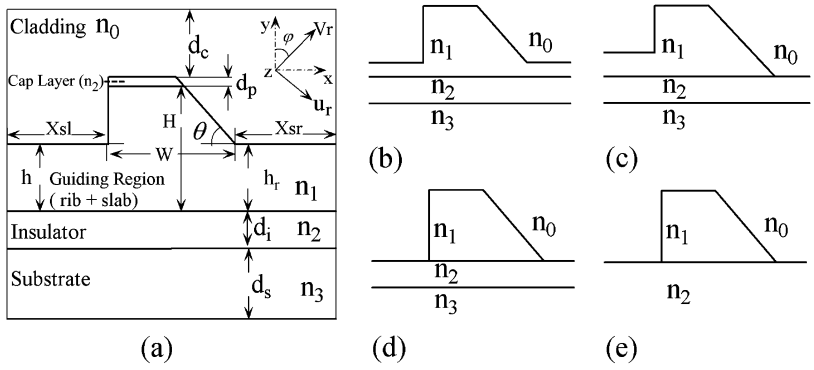


Fig. 1. Slanted-angle polarization rotator: (a) general geometry; (b) conventional symmetric external waveguiding layer design ($h_r = h$); (c) asymmetric external layer design ($h_r = 0$); (d) design without external layers; and (e) single substrate waveguide without external layers.

rib height as $r = h/H$ and the ratio of the rib width to rib height $s = W/H$ while the optical-axis rotation angle φ is taken to be positive for a clockwise rotation. For an SOI waveguide, the rib, substrate, and insulator indexes are $n_1 = n_3 = 3.48$ for silicon and $n_2 = 1.45$ for SiO_2. The wavelength $\lambda = 1.55$ μm and insulator thickness $d_i = 1.1$ μm are fixed throughout this paper.

In the asymmetric SOI design of Fig. 1(c), one of the waveguiding layers outside the rib region is etched completely to the SiO_2 layer, unlike conventional slanted-angle polarization rotators [2], [5], [6], [11]–[14] for which the external waveguiding layers are of the same height (although departures from symmetry caused by fabrication error occur, yielding undesired performance variations). Eliminating both external waveguiding layers [7], [9], [10] of course fully avoids such fabrication difficulties but at the cost of a small device cross section for single-mode operation since higher order modes then cannot radiate laterally. In this paper, we demonstrate that the single-mode region of slanted-facet waveguides, and especially waveguides with asymmetric external layers, can encompass a larger region of waveguide parameters than conventional structures, increasing fabrication tolerance.

III. Numerical Technique

While as noted in the introduction, many simulation procedures have been applied to slanted-angle waveguides, certain difficulties have been noted. The FDM, for example, can give rise to spurious modes [16], [17] and numerical instabilities [6]. Further, the procedure is relatively computationally inefficient for slanted-angle waveguides [9], [10] and possesses large errors at high-contrast waveguide corners such as those present in Fig. 1 of [7]. In contrast, the FEM, possibly enhanced through an unstructured mesh with adaptive refinement, can be easily applied to waveguide corners and slanted facets without an appreciable increase in either memory usage or CPU time. We have therefore developed a full-vectorial FEM eigenmode solver with mixed triangular elements, which employs both nodal and edge elements to solve the eigenvalue equation [18]–[20]

$$[K]\{\phi\} - \beta^2[M]\{\phi\} = \{0\}. \tag{2}$$

Here, $\{0\}, \beta$, and $\{\phi\}$ represent the null vector, modal propagation constant, and the E or H vector for the electric- and magnetic-field formalisms, respectively. The associated sparse symmetric matrices $[K]$ and $[M]$ are given in [18]–[20]. Here, we employ the H-formulation as the magnetic-field components are naturally continuous across dielectric interfaces. Through comparisons with commercial FEMLAB software from Comsol, Inc., we have found that our calculations employing 6000 mixed elements are as accurate as those obtained from the FEMLAB 2.3 package with 60 000 nodal elements and adaptive mesh refinement.

IV. Design Procedure

In this and the following sections, we examine the dependence of both the conversion efficiency between the incoming TE and TM modes and the parameter limits for single-mode operation on the details of the device geometry for slanted-angle wavelength converters. We present both descriptive two-dimensional (2-D) contour plots and simple empirical formulas from which the optimal waveguide parameters can be immediately obtained.

A. Optical-Axis Rotation Contours

In our first set of simulations, we examine the rotation of the optical axis as a function of the height and width of the slanted-angle rib waveguide as well as the thicknesses of the slab layers on both sides of the rib. The direction of the slanted waveguide facet naturally follows the (111) crystal plane. Subsequently, in our magnetic-field formulation, the rotation of the optical axis is identified with a suitable ratio of the TE and TM components of the lowest order waveguide eigenmode. In the magnetic case, three possible criteria are the vectorial ratio of the x- and y-field components $[H_x]/[H_y]$ [11], [12], the ratio of the maximum values of the x and y magnetic-field components $\max(H_x)/\max(H_y)$ [11], or the rotation parameter R [5]

$$R = \frac{\iint\limits_{\Omega} n^2(x,y) \cdot H_x^2(x,y)\, dx\, dy}{\iint\limits_{\Omega} n^2(x,y) \cdot H_y^2(x,y)\, dx\, dy} \tag{3}$$

where $n(x,y)$ is the refractive-index distribution, and the magnetic-field components $H_x(x,y)$ and $H_y(x,y)$ are the components of the specified eigenmode in the lateral and transverse directions, respectively. For a 45° optical-axis rotation, these components are almost identical so that $R = 1$.

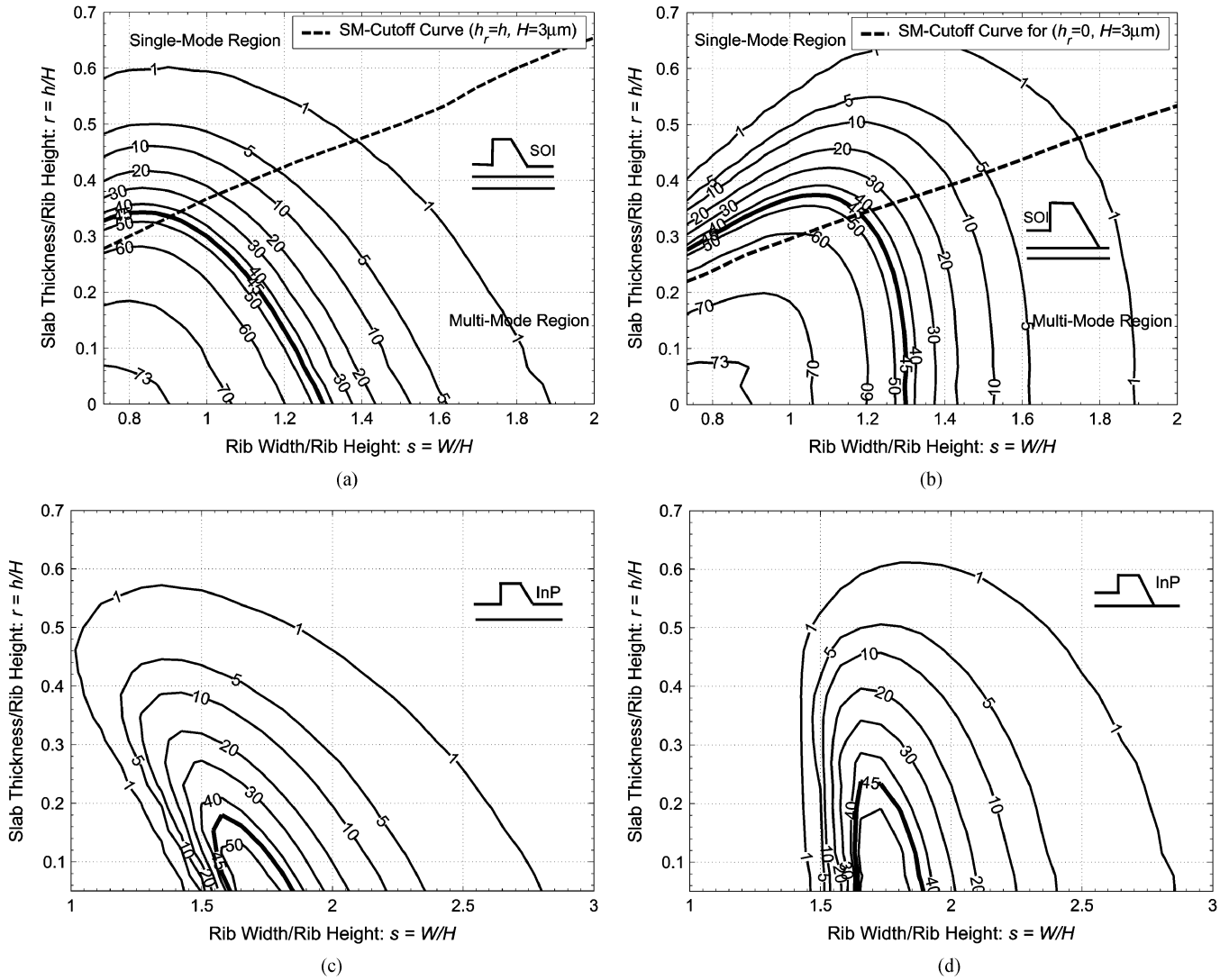


Fig. 2. Optical-axis rotation angle (φ) contours for slanted-angle waveguides: (a) symmetric external waveguiding layer SOI waveguide; (b) asymmetric waveguiding layer SOI waveguide; (c) symmetric waveguiding layer III–V waveguide ($H = 1.3\,\mu$m, $n_1 = 3.370, n_2 = n_3 = 3.324$, and $\theta = 52°$); and (d) asymmetric waveguiding layer III–V waveguide ($H = 1.3\,\mu$m, $n_1 = 3.370, n_2 = n_3 = 3.324$, and $\theta = 52°$). These III–V waveguides are single mode for $\varphi = 45°$.

In this paper, the rotation parameter is employed to characterize the optical-axis rotation as (3) contains contributions from the entire field region. The rotation parameters for the two lowest order eigenmodes are denoted as R_1 and R_2, respectively, while R without a subscript indicates R_1. Thus, $R \gg 1$ designates an x-polarized lowest order mode, while $R \ll 1$ corresponds to a y-polarized mode. Since the modes are orthogonal, the optical-axis rotation angle is

$$\varphi = \tan^{-1}(R) = \tan^{-1}(R_1) = \cot^{-1}(R_2). \qquad (4)$$

In Fig. 2, we present normalized contours for the optical-axis rotation angle as a joint function of both the normalized rib waveguide height and external waveguiding layer thickness. These contours show very low sensitivity to the silicon film thickness H for $1\,\mu\text{m} < H < 30\,\mu\text{m}$. The different cases in the figures are as follows: Fig. 2(a) corresponds to a conventional symmetric external waveguiding layer SOI polarization rotator, Fig. 2(b) to our proposed slanted-angle asymmetric external waveguiding layer SOI design, Fig. 2(c) to a conventional 1.3-μm weakly guided InGaAsP waveguide [6], [11], and Fig. 2(d) to an InGaAsP rotator with an asymmetric waveguiding layer geometry, and $n_1 = 3.370$ in the rib, $n_2 = n_3 = 3.324$ in the substrate, and a facet angle of $\theta = 52°$.

Besides being nearly independent of the silicon layer thickness, the information in Fig. 2 can be employed for both single- and multiple-section rotators. That is, any waveguide that exhibits a 45° optical-axis rotation can be employed as a single-section rotator, while, e.g., a 22.5° polarization-rotating waveguide is suitable for a two-section rotator (compare with [5, eq. (2)]). As we focus here on single-section components for reasons of size, loss, and fabrication simplicity, the 45° contour is distinguished in the graphs by its thickness. The two dashed lines in Fig. 2(a) and (b) indicate the waveguide parameters corresponding to the single-mode cutoff condition and will be discussed in detail in Section V.

To establish the accuracy of our results, we observe from Fig. 2(c) that a $H = 1.3$-μm single-section III–V rotator rib

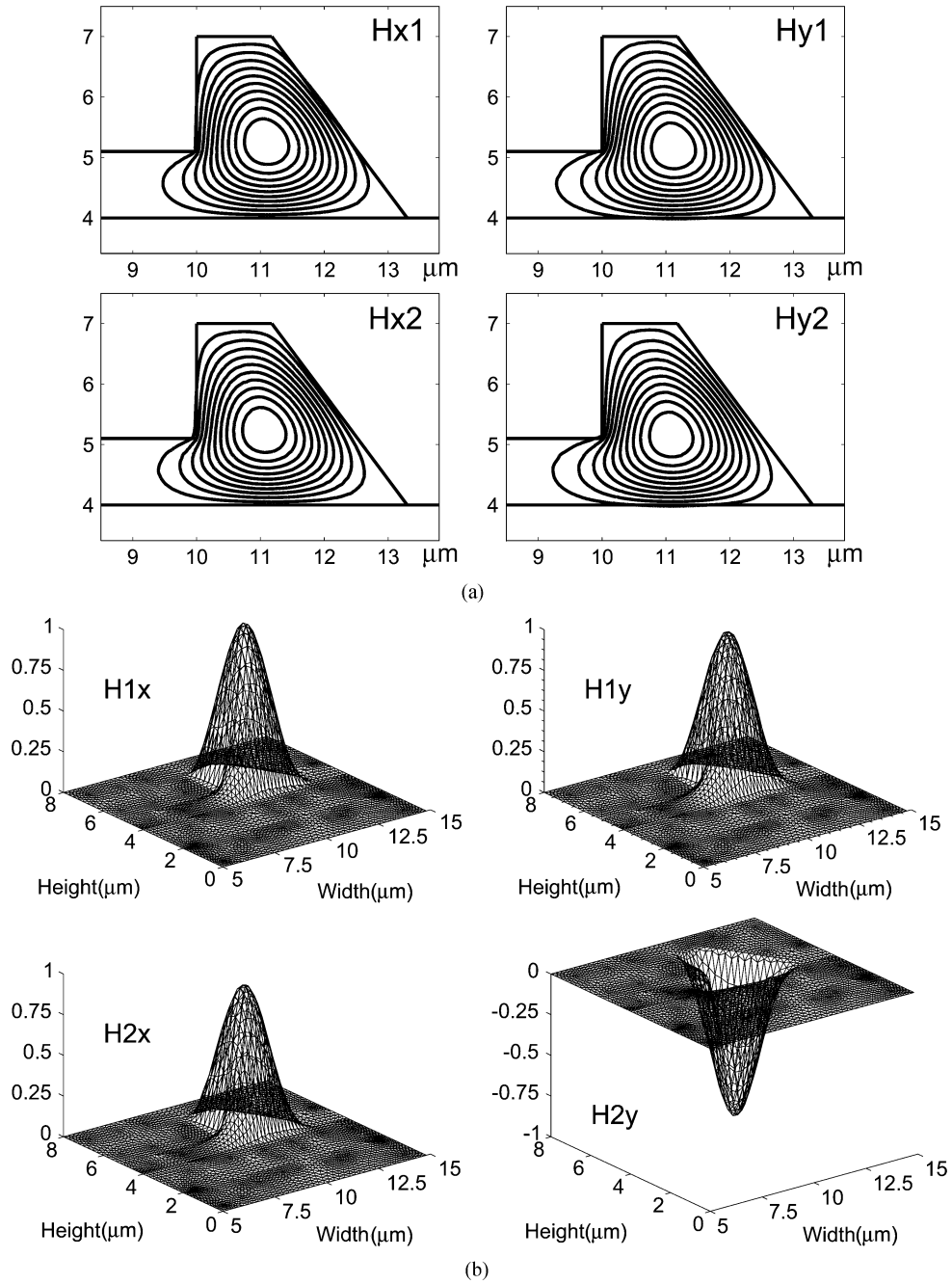


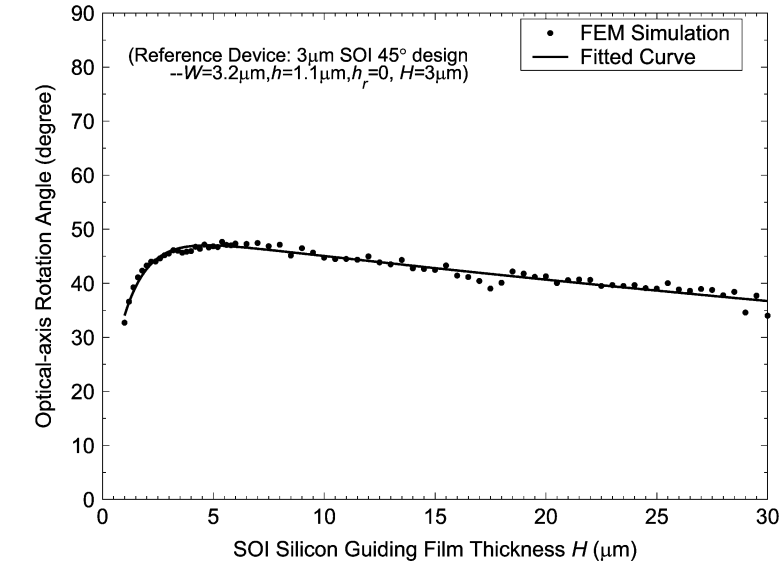
Fig. 3. Orthogonally polarized two lowest order modes of a $\varphi = 45^\circ$ SOI waveguide with $h = 1.1$ μm, $W = 3.3$ μm, $H = 3$ μm, $h_r = 0$, $L_\pi = 850$ μm, and $R = 1.07$: (a) 2-D contour graph and (b) three-dimensional (3-D) surface plot.

width requires a waveguide width $W = 2.4$ μm for a height of $h = 0.1$ μm. This result agrees with the published value of $\sim$2.5 μm ([6, Case 1 of Table I], [11, Fig. 4], [15, Fig. 7]); however, [11, Fig. 5] indicates that the maximum field ratio (H_x/H_y or H_y/H_x) occurs at $W = 2.4$ μm. Our graph additionally yields a continuum of design parameters and explains previous observations such as the increase and the subsequent decrease of hybridization with increasing rib width ([12, Fig. 2]) as verified from the rotation angles along lines of constant h in Fig. 2(c).

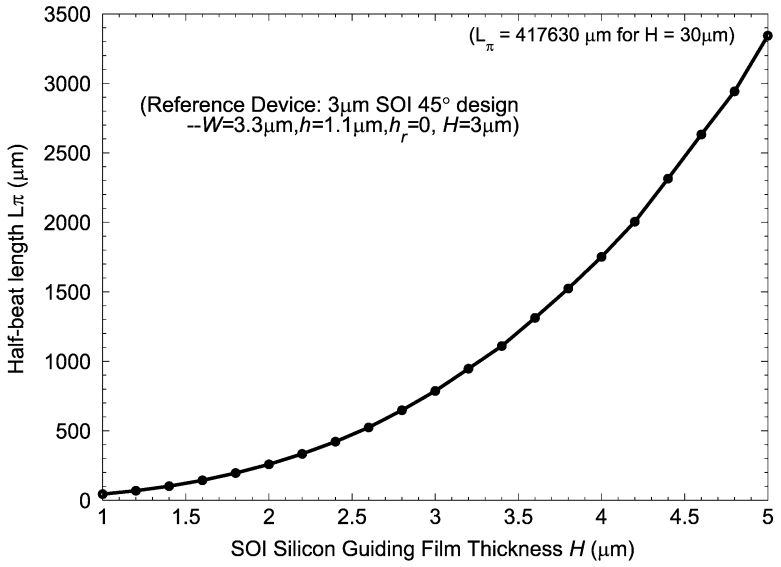
B. SOI Waveguide Analysis

To illustrate our design procedure through a practical example, we consider the single-section SOI polarization-rotating waveguide given by $h = 1.1$ μm, $W = 3.3$ μm, $h_r = 0$, and $H = 3$ μm, which is located on the 45° contour line and in the single-mode region of Fig. 2(b). The two lowest order eigenmodes of this waveguide are shown in Fig. 3. Observe that the two eigenmodes are almost identical as required for a 45° optical-axis rotation. The length of the corresponding polarization rotator is $L_\pi = 850$ μm.

The additional range of parameter choices provided by SOI waveguides compared with low-index-contrast III–V waveguides is evident from the lengths of the 45° contours in Fig. 2(a)–(d). Thus, while the 3-μm SOI rotator mentioned in the previous paragraph has a length of 850 μm (which is close to the reported value of $\sim$700 μm for equivalent 1.3-μm



(a)



(b)

Fig. 4. (a) The optical-axis rotation angle φ and (b) the half-beat length L_π for similar asymmetric waveguiding layer waveguides as a function of SOI silicon layer thickness H where $r = h/H, s = W/H$ and h_r/H are kept invariant.

III–V rotators [6], [11]), we have found that single-mode 1.3-μm SOI structures can be designed with L_π between 35 and 100 μm, yielding much shorter device lengths. To illustrate, a single-mode waveguide with $H = 1.3$ μm, $h = 0.4$ μm, $W = 1.55$ μm, and $h_r = 0$, yields $R = 1.02$ and a half-beat length $L_\pi = 98$ μm, while a waveguide with $H = 1.3$ μm, $h = 0.35$ μm, $W = 0.95$ μm, and $h_r = 0$ has $R = 0.98$ and $L_\pi = 34$ μm.

Another feature of our SOI waveguide design is the large cross section, which can easily be made comparable to single-mode-fiber diameters, reducing coupling loss. Further, the field is effectively confined to the rib, unlike III–V waveguides, which generally require a thick (> 5 μm) substrate [8]. For larger waveguides, fabrication tolerance is enhanced while the strong optical confinement decreases the optical loss, minimum bending radius, and device spacing. Together with the decreased substrate thickness, these SOI designs indicate that compact and low-price products can be fabricated, which are fully compatible with complementary metal–oxide–semiconductor (CMOS) integrated circuit (IC) technology.

C. Range of Validity

While the contour charts of Fig. 2(a) and (b) were calculated for a $H = 3$-μm silicon-guiding-layer thickness, almost identical results are obtained for a wide range of Si thicknesses. As the contour lines are almost invariant for $H = 2$ and 5 μm, we do not display these graphs separately but instead normalize the geometric parameters W and h with respect to the silicon film thickness H. In this section, we therefore study the range of H values for which such a normalization yields nearly equivalent curves.

We first select a $\varphi = 45^\circ$ asymmetric-waveguiding-layer structure of Fig. 1(c) with $W = 3.2$ μm, $h = 1.1$ μm, $h_r = 0$, and $H = 3$ μm as a reference waveguide and then display in Fig. 4(a) and (b) our FEM results for the optical-axis rotation and the half-beat length as H is varied from 1 to 30 μm, while

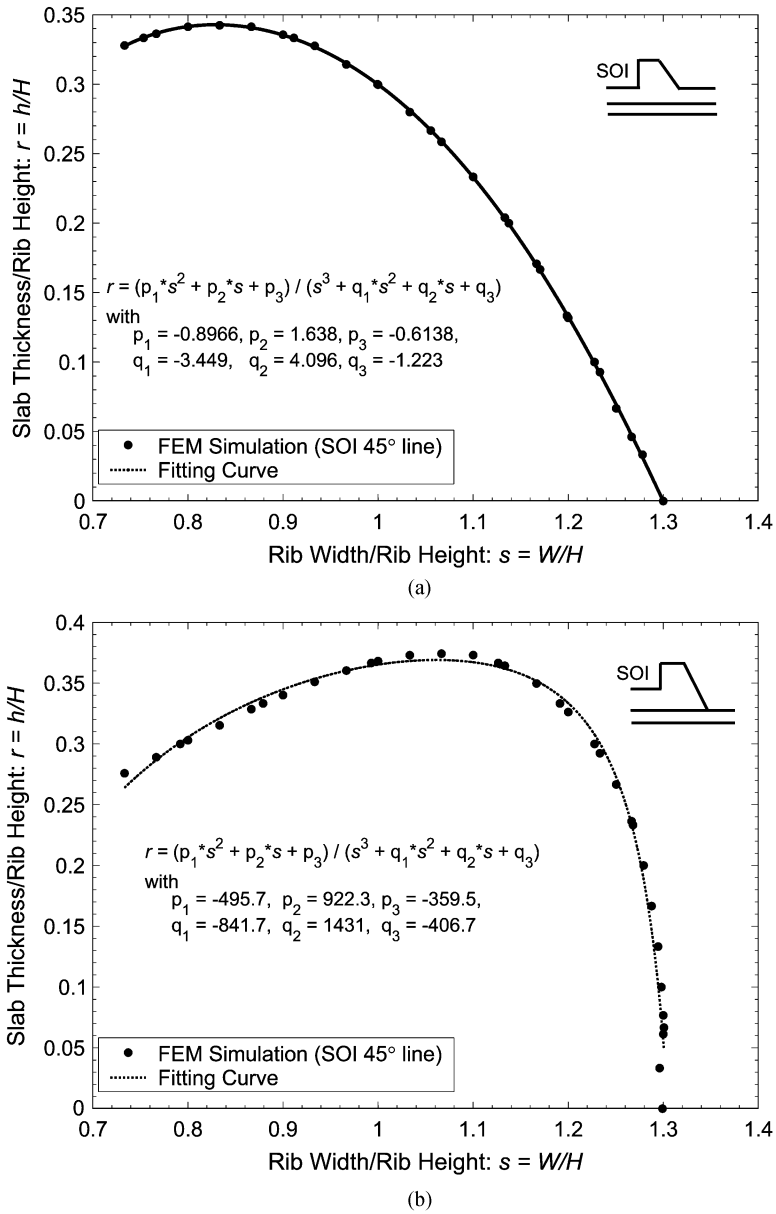


Fig. 5. 45° optical-axis rotation contours of Fig. 2(a) and (b) together with a rational polynomial approximation for (a) a conventional symmetric-external-waveguiding-layer SOI structure and (b) our asymmetric-layer SOI structure.

$r = h/H, s = W/H$, and h_r/H are kept invariant. Note that the optical-axis rotation is nearly independent of the silicon layer thickness H in this region, and in fact for $2\ \mu\text{m} < H < 10\ \mu\text{m}$ the rotation angle φ varies by only 1°. The 8° decrease in rotation angle at $H = 30\ \mu$m can be compensated by reducing W by $< 10\%$ of H, as is evident from Fig. 2(b). To obtain approximate parameters for a 45° optical-axis rotating waveguide, our normalized charts can accordingly be applied to any commercially available wafer with $1\ \mu\text{m} < H < 30\ \mu$m. However, since the half-beat length, compare Fig. 4(b), increases exponentially with H, for short devices H should be minimized.

That the optical-axis rotation remains nearly constant as the SOI waveguide dimensions are varied can be understood from the field distributions of Fig. 3. Since these are almost fully contained in the rib waveguide, they are influenced to almost the same degree by the SOI waveguide geometry. Hence, the modes are equally TE or TM with respect to the slanted waveguide facet. In contrast, in a standard III–V semiconductor waveguide, the depth of penetration of the modal field (as evident from, e.g., [5, Fig. 6], [11, Fig. 4], and [15, Fig. 9]) into the substrate region varies rapidly with changes in the waveguide dimension so that the overall shape of the field and hence the hybridization induced by the slanted facet changes rapidly with guiding-layer thickness.

D. Simplified SOI Design Expression

While Fig. 2 can be employed to design arbitrary single or multiple-section polarization rotators, for a single-section device only the 45° contour is of practical interest. This contour can be approximated by a simple rational polynomial

$$r = \frac{p_1 \cdot s^2 + p_2 \cdot s + p_3}{s^3 + q_1 \cdot s^2 + q_2 \cdot s + q_3} \tag{5}$$

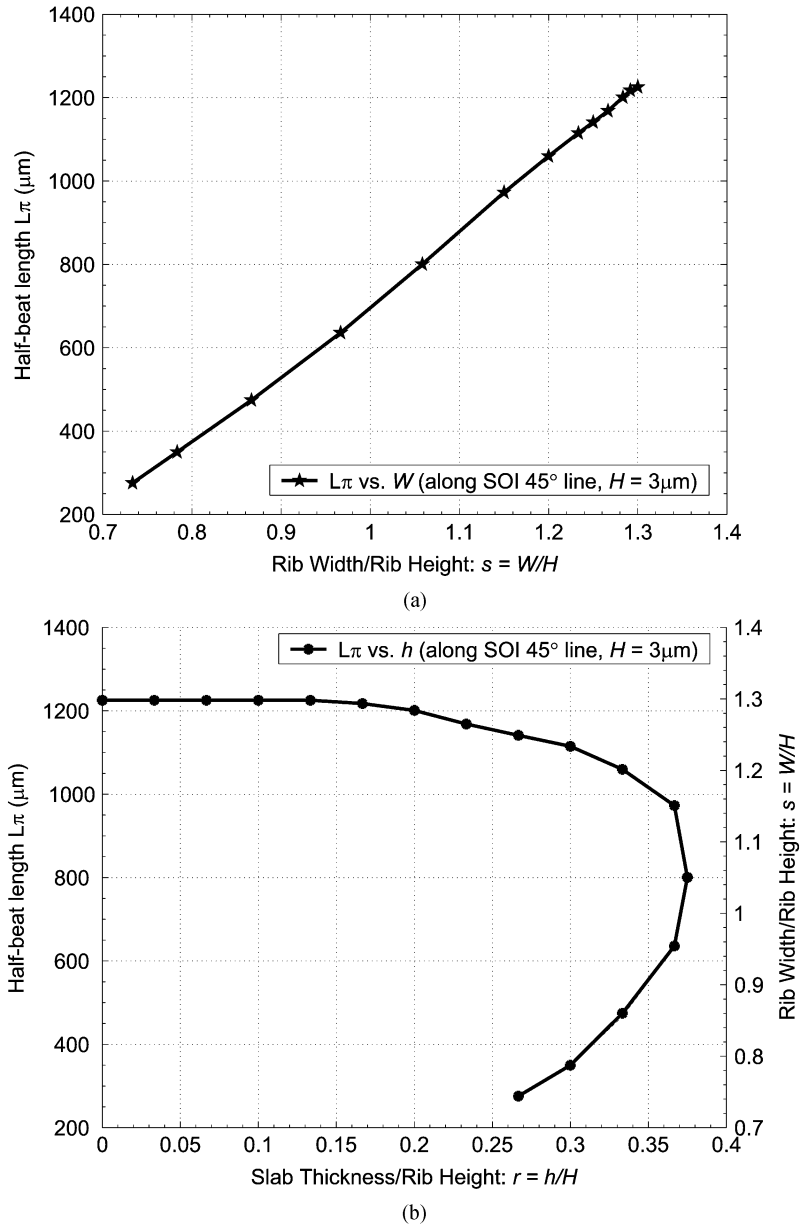


Fig. 6. Dependence of the half-beat length L_π for asymmetric-external-waveguiding-layer waveguides that rotate the optical axis by 45° with (a) rib width W and (b) external-waveguiding-layer height h.

with $r = (h/H)$ and $s = (W/H)$ as demonstrated in Fig. 5(a) and (b). Equation (5) fits other rotation-angle contours as well. For single-section rotators, the coefficients appearing in (5) are $p_1 = -495.7, p_2 = 922.3, p_3 = -359.5, q_1 = -841.7, q_2 = 1431$, and $q_3 = -406.7$ for the asymmetric-external-waveguiding-layer SOI structure of Fig. 1(c), and $p_1 = -0.8966, p_2 = 1.638, p_3 = -0.6138, q_1 = -3.449, q_2 = 4.096$, and $q_3 = -1.223$ for the conventional-symmetric-external-waveguiding-layer SOI structure of Fig. 1(b). Following the considerations of the previous section, these parameters were determined for a 3-μm SOI silicon film thickness but can be applied to a good approximation within the range 1 μm $< H <$ 30 μm.

E. Half-Beat Length Variation

Finally, we determine the device length as a function of the rib-waveguide dimension for a single-section polarization rotator. We display in Fig. 6(a) and (b) the variation of the half-beat length L_π with the rib base width W and the external-waveguiding-layer thickness h, respectively, for asymmetric-external-waveguiding-layer SOI waveguides on a 3-μm Si guiding layer that exhibits a 45° optical-axis rotation. Clearly, the half-beat length L_π varies linearly with rib width W but reflects the path of the 45° contour in Fig. 5(b) with the slab thickness h. From this behavior, together with the exponential relationship in Fig. 4(b), the device length can be estimated for any waveguide. In particular, for an Si film thicknesses of 1.3, 2, 3, and 5 μm, we found that, respectively, 35 μm $\leq L_\pi \leq$ 100 μm, 125 μm $\leq L_\pi \leq$ 375 μm, 250 μm $\leq L_\pi \leq$ 1225 μm, and 1150 μm $\leq L_\pi \leq$ 5125 μm. In each of these cases, L_π varies linearly with rib width as in Fig. 6(a), and with slab thickness in the same manner as in Fig. 6(b). Evidently, a 3-μm Si guiding layer encompasses L_π values

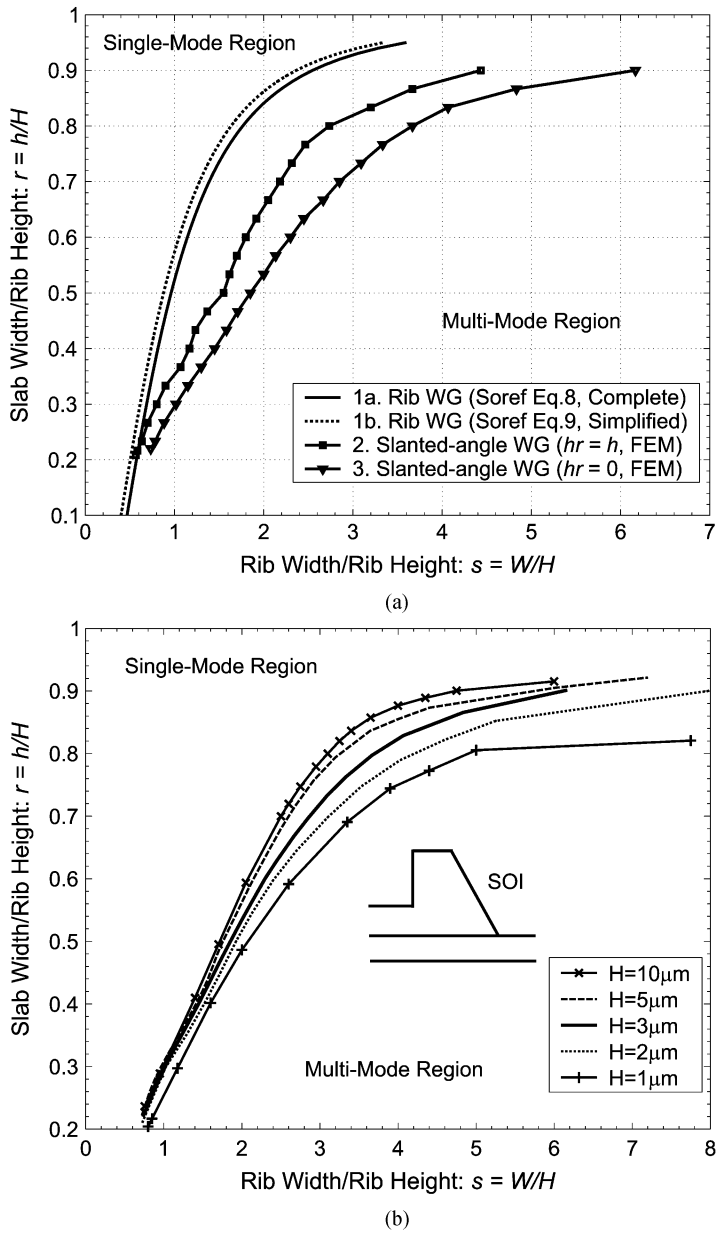


Fig. 7. Single-mode region boundary for (a) the SOI rib waveguide and slanted-angle polarization rotators with same silicon film thickness $H = 3\ \mu$m and (b) the asymmetrical-external-waveguiding-layer waveguides with different silicon guiding-film thicknesses.

that are relevant to most practical applications, while extremely short (35–100-μm) SOI polarization rotators can in principle be designed (compare Section IV-B) with the same 1.3-μm cross section as many current III–V rotators, which typically are several hundred micrometers in length.

V. Single-Mode Condition

Low-loss, high-conversion-efficiency polarization rotators must support a single guided mode for each polarization in order to insure that no power is coupled into higher order modes during propagation. The condition for single-mode operation can be simply approximated by Soref's formulas for SOI rib waveguides [21]–[23], but this expression is invalid for slanted-angle waveguides where modes become strongly hybridized. In addition, previous studies were limited to slightly etched SOI rib waveguides with $0.5 < r = h/H < 1$, although strong polarization conversion instead requires deeply etched waveguides with $0 < r < 0.5$, as evident from Fig. 2. While Pogossian [23] modified Soref's formula to improve its relevance to waveguide design, his expression is based on data [24] generated from Soref's original formula [21]. Similarly, the single-mode simulations of [22] employ numerical procedures for weakly guiding structures, while [25] mistakes the deep-etching $(r \leq 0.5)$ for Soref's shallow-etching $(r \geq 0.5)$ condition.

Here, we determine the single-mode cutoff condition through an FEM mode solver by increasing the rib width for a fixed slab thickness until a third mode appears. First, we contrast in Fig. 7(a) the single-mode cutoff of different waveguides with the same silicon film thickness $H = 3\ \mu$m. The curves marked 1–3 correspond to standard rib waveguides, symmetric-external-waveguiding-layer, and asymmetric-external-layer

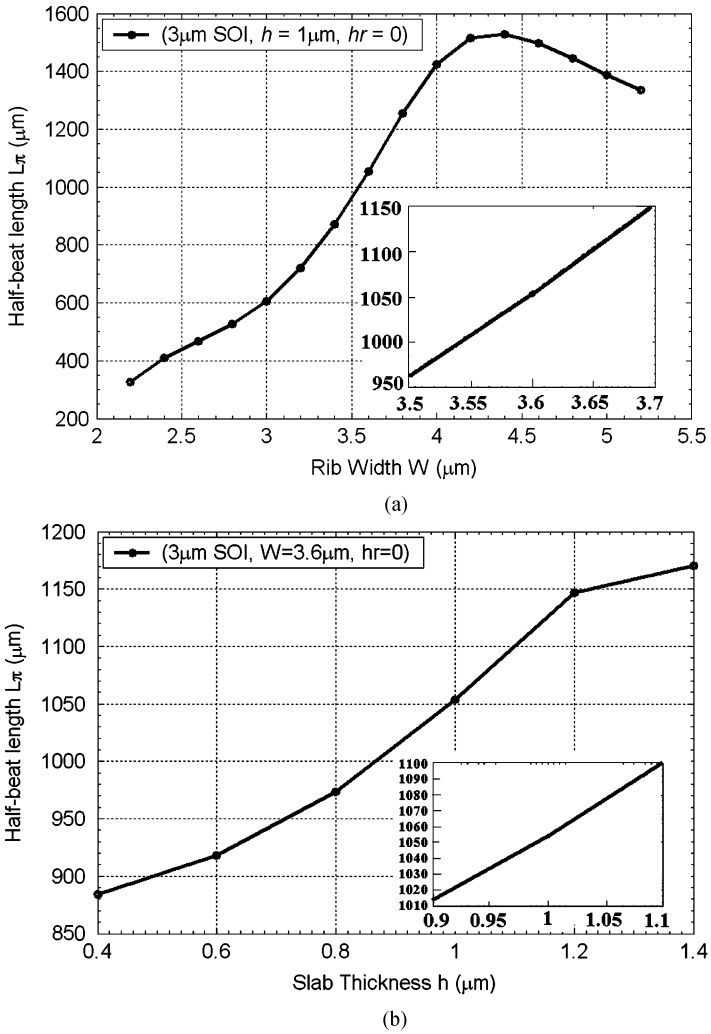


Fig. 8. Variation of the half-beat length L_π with respect to the (a) width W of the base of the rib for an external-waveguiding-layer thickness for $h = 1$ μm and (b) h for $W = 3.6$ μm.

slanted-angle waveguides, respectively. The FEM simulation clearly verifies that Soref's formulation [21, eq. (8) and (9)] is the most accurate formulation for SOI rib waveguides. From Fig. 7(a), we conclude that for a fixed silicon film thickness H, our asymmetric external layer design displays the greatest region of waveguide parameter space (r, s) for single-mode operation. At a fixed value of $r = h/H$, the asymmetric-waveguiding-layer slanted-angle structure of Fig. 1(c) provides the largest range of normalized widths $s = W/H$ that yield a single-mode waveguide with a 45° optical-axis rotation.

Next, we examine in Fig. 7(b) the single-mode behavior of our asymmetric-waveguiding-layer structure as the silicon-layer thickness H is varied. As expected, as the thickness is decreased, a larger region of parameter space is associated with single-mode behavior. On the other hand, to achieve a large optical-axis rotation, the waveguide must be deeply etched, as evident from Fig. 2. The single-mode boundary curve is then nearly invariant even with respect to changes in the silicon-layer thickness H.

Consequently, although the single-mode boundary curves in Fig. 2(a) and (b) are computed with $H = 3$ μm, these curves are nearly unchanged for 1 μm $< H <$ 30 μm, varying by less than 1% for $r < 0.5$. In contrast, for the $H = 1.3$ μm III–V devices discussed in Fig. 2(c) and (d), all waveguides that rotate the optical axis by 45° are single mode; however, the single-mode behavior of III–V waveguides is dependent on H, as discussed in Section IV-C. Referring to Fig. 2(a) and (b), a 45° optical-axis-rotating single-mode SOI waveguide requires $0.2 < r < 0.4$. Any point on the 45° optical-axis rotation contour therefore yields a realizable single-section polarization rotator, as typified by Fig. 3.

As well, Fig. 2(a) and (b) indicates that the asymmetric-waveguiding-layer structure has an enhanced region of single-mode operation given by $1.2 > s = W/H > 0.71$, while the corresponding interval for the symmetric external layer structure is $0.9 > s > 0.71$. Coupled with the ease of fabrication of structures for which an SiO_2 insulator layer prevents further etching of the slanted facet, our results clearly indicate the potential advantages of the asymmetric structure.

VI. Fabrication Tolerance

In this section, we analyze the fabrication tolerance of the asymmetric-external-waveguiding-layer waveguide of Fig. 1(c).

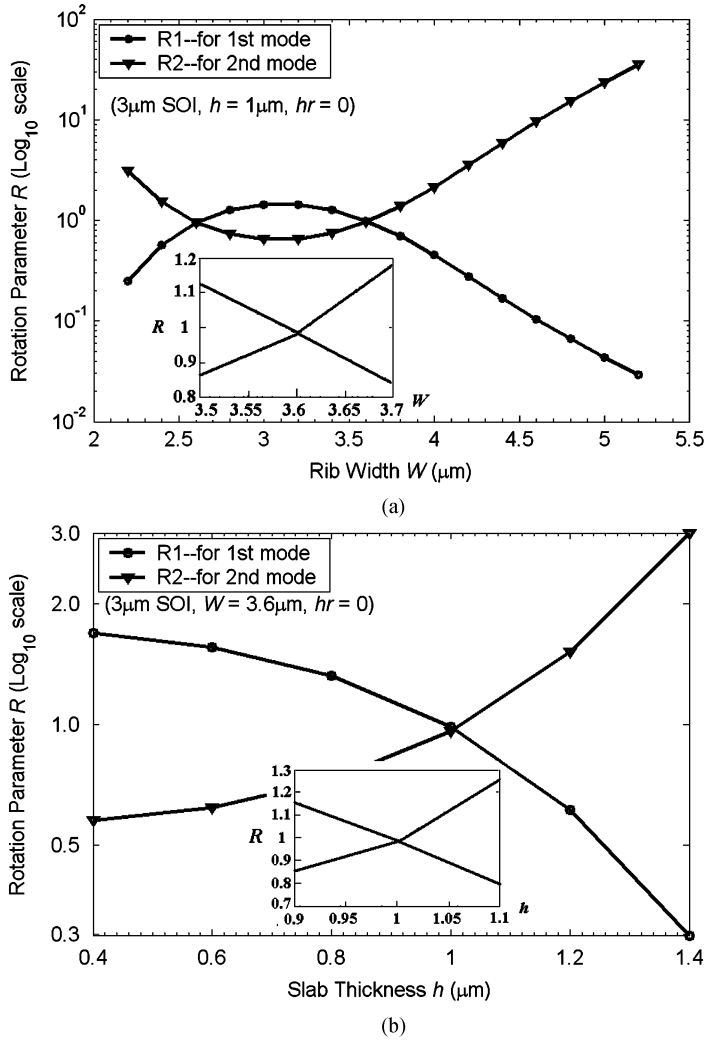


Fig. 9. Optical-axis rotation parameters R_1 and R_2 as a function of (a) the width W of the rib base for an external-waveguiding-layer thickness $h = 1$ μm and (b) the external layer thickness h for a rib base width $W = 3.6$ μm.

The conversion efficiency of a polarization rotator is principally limited by fabrication errors that we model here by assuming 0.1-μm fluctuations in design parameters as typically encountered in low-cost silicon processing [27].

For example, a thick silicon layer (e.g., $H = 10$ μm) has a greater tolerance than a thin layer (e.g., $H = 3$ μm) to a 0.1-μm parameter change. However, even for the same silicon film thicknesses, the fabrication tolerance varies moderately with the location of the waveguide design on the 45° line of our contour plots. A complete study of the fabrication tolerance of commercial SOI wafers is therefore beyond the scope of this paper and will be presented elsewhere.

To illustrate the magnitude of fabrication tolerances, we first consider a waveguide with $H = 3$ μm, $h_r = 0, h = 1$ μm, and $W = 3.6$ μm, which yields a half-beat length $L_\pi = 1053.5$ μm for a 45° optical-axis rotation according to Fig. 2(c). We also describe the variation of the optical-axis rotation parameter R and half-beat length L_π with rib width W and external-waveguiding-layer thickness h. Varying W from 2.2 to 5.2 μm yields Figs. 8(a) and 9(a) for L_π and R. The dependence of these quantities on h for $0.4 < h < 1.4$ μm is instead displayed in Figs. 8(b) and 9(b). From Fig. 8(a) and (b), we find that a 0.1-μm fabrication error in W or h changes L_π by 80 and 40 μm, respectively. These values compare with 50 and 20 μm for the corresponding III–V waveguide with $L_\pi = 403$ μm given by [12, Figs. 2 and 10]. However, the relative deviation $(\Delta L_\pi)/(L_\pi) \times 100\%$ in the SOI case is 7.6% and 3.8%, which is markedly smaller than 12.4% and 5% for the III–V waveguide in [12].

From Fig. 9(a) and (b), we observe additionally that the rotation parameters R_1 and R_2 are inversely proportional to each other. The reciprocal relationship is a direct consequence of the orthogonality of the two lowest order modes. From Fig. 9 and (4), the maximum variation of the optical-axis rotation angle φ is bounded by $+4^\circ$ when either the rib width or the rib height is reduced by 0.1 μm and by -7° when W or h is increased by 0.1 μm.

More closely related to device performance are the polarization conversion (PC) efficiency and the polarization extinction ratio (ER). The first of these measures the percentage of power P transferred between the orthogonal polarization components for a given input polarization state and is therefore $\mathrm{PC}_{\mathrm{TE}\to\mathrm{TM}} = P_{\mathrm{TM}}/(P_{\mathrm{TE}} + P_{\mathrm{TM}}) \times 100\%$ for an incoming TE mode. After some algebraic manipulations, the PC is found

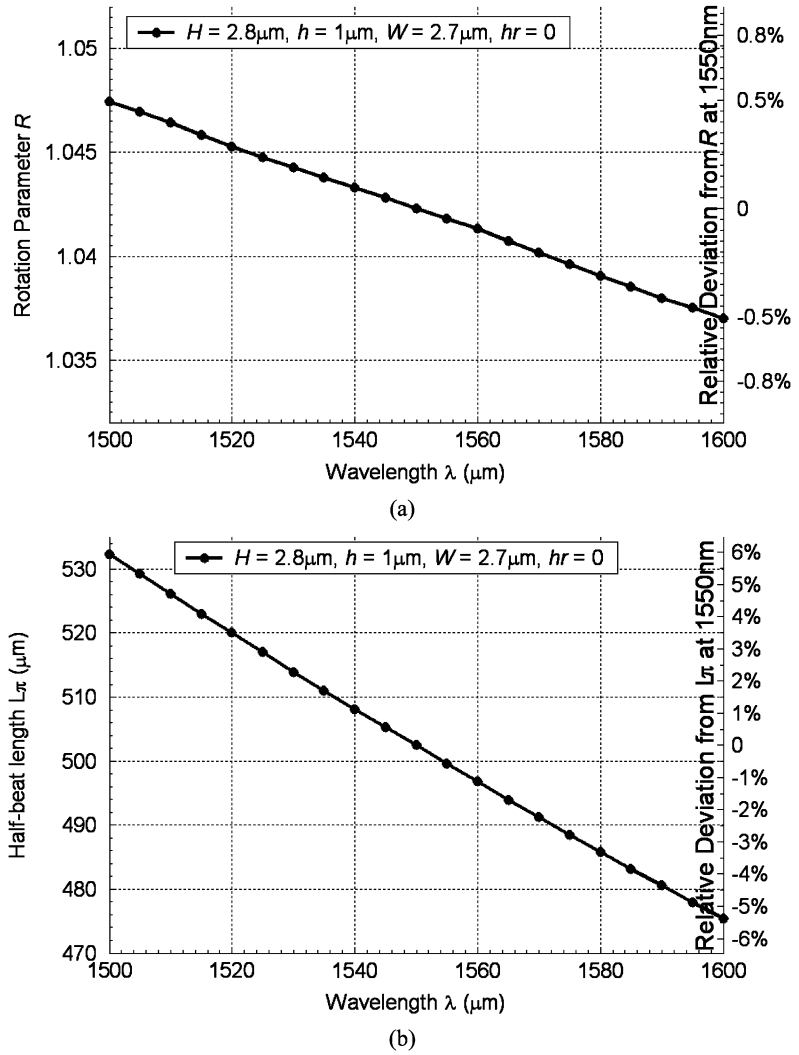


Fig. 10. Wavelength dependence of (a) the rotation parameter (optical-axis rotation angle) and (b) the half-beat length (required device length).

to be in terms of the device length L, half-beat length L_π, and rotation parameter R or optical-axis rotation angle φ (this equation is readily verified from the BPM data for InGaAsP devices presented for $\lambda = 1.61$ μm in [12, Figs. 12 and 13], [7, Fig. 3], and [3, Fig. 6 of ref. [7]]), as follows:

$$\mathrm{PC} = 4\sin^2\varphi\cos^2\varphi\sin^2\left(\frac{\pi L}{2L_\pi}\right)\times 100\% \qquad (6)$$

while the ER, which is related in the absence of loss to the polarization conversion efficiency by $\mathrm{ER} = 10\log[(1-\mathrm{PC})/\mathrm{PC}]$, is defined as [10], as follows:

$$\mathrm{ER} = 10\log\left(\frac{P_{\mathrm{TE}}^{\mathrm{out}}}{P_{\mathrm{TM}}^{\mathrm{out}}}\right)\Bigg|_{\mathrm{TE-polarized\,input}} \quad (\mathrm{dB}). \qquad (7)$$

For our 3-μm SOI rotator test case, PC $= 99.98\%$ and ER $= -38$ dB. Even for a variation of W of 0.1 μm, which yields the maximum -7° rotation angle variation, we calculate $\Delta L_\pi = 7.6\%$ and PC $= 92.81\%$ corresponding to ER $= -11$ dB, while a 0.1-μm h variation yields $\Delta L_\pi = 3.8\%$, PC $= 97.71\%$, and ER $= -16$ dB. In both of these worst cases, the performance is acceptable for many applications (compare with [10, Fig. 5], and PC $= 92 \sim 93\%$ after ± 0.1-μm rib width variation in [5]).

Repeating the above analysis for a 1.3-μm SOI rotator with $h_r = 0, h = 0.4$ μm, $W = 1.55$ μm, and $L_\pi = 98$ μm, we find that the dependence of L_π and R on W and h is largely identical to Figs. 8 and 9. While the fabrication tolerances are decreased relative to the 3-μm rotator since PC $= 87.59\%$ and ER $= -8.5$ dB for $\Delta W = 0.1$ μm, while PC $= 93.07\%$ and ER $= -11.3$ dB for $\Delta h = 0.1$ μm, the conversion efficiencies improve to PC $= 96.15\%$ and ER $= -14$ dB for $\Delta W = 0.05$ μm, while PC $= 97.62\%$ and ER $= -16$ dB for $\Delta h = 0.05$ μm. These compare favorably to the conversion values of 80% in a 0.3-mm device of [1] and 85% and 45% in [4]. Since the modes of the SOI waveguides are highly confined and are therefore more influenced by geometric variations, the fabrication tolerance of the SOI rotator is slightly less than that of InGaAsP converters with equivalent guiding-layer thicknesses (compare with [10, Fig. 5]). However, ultracompact SOI devices are more easily fabricated than similar III–V structures, which can possess certain dimensions below 50 nm (compare with [1, Fig. 2] and [3, Fig. 1] where $L_\pi = 230$ μm). Improved silicon fabrication methods with 0.05-μm resolution, possibly involving

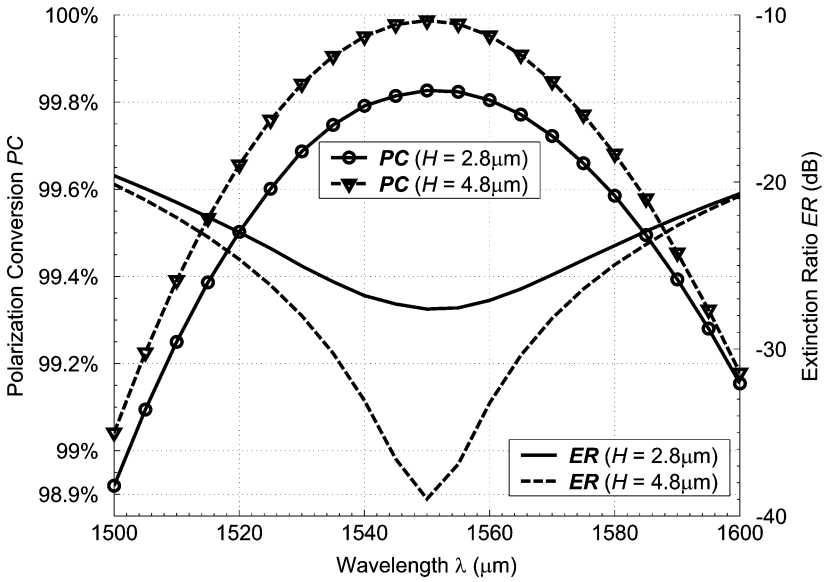


Fig. 11. Wavelength dependence of the PC efficiency and polarization ER for the 3- and 5-μm designs.

nanotechnology, should result in ultrashort polarization rotators with conversion efficiency >96%.

VII. Spectral Properties

To determine the applicability of the polarization rotator design to wavelength-division-multiplexing (WDM) systems, we now study the behavior of two representative devices in the C band (1528.77–1563.86 nm) and L band (1573.71–1604.03 nm), as defined by the International Telecommunications Union Telecommunication Standardization Sector (ITU-T) G.692 standard. These are a 3-μm design with $H = 2.8$ μm, $h = 1$ μm, $W = 2.7$ μm, $h_r = 0, R = 1.04$, and $L_\pi = 502.4$ μm and a 5-μm design with $H = 4.8$ μm, $h = 1.8$ μm, $W = 4.8$ μm, $h_r = 0, R = 1.01$, and $L_\pi = 2572$ μm. The geometric parameters are rounded to the nearest tenth of a micrometer, which models the fabrication precision. Further, the values of H are reduced by 0.2 μm from the optimal film thicknesses specified above to model the 0.2-μm silicon layer loss observed experimentally after removing the top protecting layer during fabrication [27].

In Figs. 10(a) and (b), we respectively display R and L_π as a function of wavelength for the 3-μm design. In a wavelength range of 1.50–1.60 μm, the rotation parameter R varies by $\pm 0.5\%$ from its value at 1.55 μm, corresponding to a maximum change of 0.15° in the optical-axis rotation angle, while L_π varies by $\pm 6\%$. While between 1.55 and 1.60 μm the variation of R is far smaller than the 6% predicted for the III–V converter in [12, Fig. 12], L_π varies slightly more than the 5% reported in this reference.

The PC efficiencies and crosstalk for $1.50 < \lambda < 1.60$ μm for the 3- and 5-μm components are plotted in Fig. 11. Although in principle a 3-μm rotator can display the same performance as the 5-μm device with PC = 99.98% and ER = −37 dB for 0.1-μm fabrication tolerance, the larger layer thickness is clearly preferable. That the SOI polarization converters are highly wavelength-independent is evident from PC > 99% in the $1.50 < \lambda < 1.60$ μm wavelength range while PC > 99.7% in the C band where the 3- and 5-μm components display <−25-dB and <−30-dB polarization crosstalk, respectively.

VIII. Loss Considerations

Large cross-section SOI polarization converters display reduced loss as a result of both the small measured fiber-coupling losses, e.g., 0.17 dB per facet [25], and the small material losses, which were found to be below 0.5 dB/cm for large cross-section waveguides in [24] and 0.1 dB/cm in [25]. The low coupling losses reflect both the high degree of field confinement to the guiding layer as in Fig. 3 and the large single-mode waveguide cross sections that properly match the mode- diameters of standard single-mode fibers [8], [21]–[25].

While a full discussion of losses of SOI polarization rotators requires a detailed analysis and will therefore be considered in a forthcoming paper, our SOI polarization rotator designs display low insertion loss. For example, taking into account only the calculated modal field overlaps, the coupling between our asymmetric-external-layer SOI polarization converter with $h_r = 0$ and a Corning SMF-28 fiber with a core diameter of 8.3 μm and core and cladding indexes of 1.5362 and 1.5306 is 0.5 dB for $(H, h, W) = (15, 5, 13)$ μm, 2 dB for $(H, h, W) = (10, 3, 8.5)$ μm, 5.7 dB for $(H, h, W) = (5, 1.8, 4.8)$ μm, and 8.7 dB for $(H, h, W) = (3, 1.1, 3.3)$ μm. This compares with our calculated value of 7 dB for the component discussed in [11] and [6]. If the converter is instead coupled to a tapered and lensed fiber which yields, for example, a spot diameter of 2.5 μm, the polarization rotator with the most closely matched field size (here the 3-μm design) will instead yield lowest loss, in this case <2 dB.

In many applications, the converter is butt-coupled to rib waveguides as in [6, Fig. 1], [7], [11], [12], and [14]. If the vertical walls of the SOI rib waveguide and the slanted-angle SOI polarization converter coincide, we obtain a minimum coupling loss of 0.2 dB for both polarizations in the 3-μm design. This is achieved for an SOI rib waveguide with the same rib height $H = 3$ μm and slab thickness $h = 1.1$ μm

and for a rib width $W_{\rm rib} = 2$ μm. As a comparison, the total insertion loss for a III–V converter is 0.5 [11] or 0.6 dB [12] in the same configuration. If we increase $W_{\rm rib}$ to 3 μm, the losses are 0.45 dB for an incoming TE mode and 0.68 dB for a TM mode.

IX. Conclusion

This paper has mapped the optical-axis rotation and single-mode cutoff condition of slanted-angle polarization rotators onto a contour map in normalized variables. For the subset of SOI slanted-angle waveguides that rotate the optical axis by 45°, the information in the 2-D diagram can be summarized by a one-dimensional empirical formula for the waveguide parameters. This procedure enables the rapid design of periodic and single-section slanted-angle polarization converters with either symmetric or asymmetric external waveguiding layers for rib heights from 1 to 30 μm. The single-mode cutoff condition of SOI structures with different silicon-guiding-layer thicknesses was also examined, and it was demonstrated that the asymmetric-slab structure has a considerably larger region of single-mode behavior, and therefore fabrication tolerance, than other waveguide designs. For the same guiding-layer thickness, SOI polarization rotators exhibit enhanced optical confinement and are therefore shorter than III–V components. In addition, such components display small coupling losses (0.2 dB), flat spectral response ($|\Delta R| < 0.5\%$ for $1.50 < \lambda < 1.60$ μm), high conversion efficiency (99.98%), and low polarization ER (-38 dB). SOI polarization rotators, which can easily be produced with electronic device fabrication technology, should therefore find numerous applications in dense-WDM systems.

While the design methodology described in this paper enables, at least in principle, the design of short polarization rotators with nearly 100% polarization conversion and an ER <-30 dB, the realization of short (<100 μm) components can require technological precision of 0.05 μm or less. Experimental verification of the results in this paper is accordingly in progress [26], [27].

Acknowledgment

H. Deng would like to thank his co-supervisor Dr. S. K. Chaudhuri for continual discussions and encouragement.

References

[1] Y. Shani, R. Alferness, T. Koch, U. Koren, M. Oron, B. I. Miller, and M. G. Young, "Polarization rotation in asymmetric periodic loaded rib waveguides," *Appl. Phys. Lett.*, vol. 59, no. 11, pp. 1278–1280, Sep. 1991.

[2] J. J. G. M. van del Tol, F. Hakimzadeh, J. W. Pedersen, D. Li, and H. van Brug, "A new short and low-loss passive polarization converter on InP," *IEEE Photon. Technol. Lett.*, vol. 7, no. 1, pp. 32–34, Jan. 1995.

[3] K. Mertens, B. Scholl, and H. J. Schmitt, "Strong polarization conversion in periodically loaded strip waveguides," *IEEE Photon. Technol. Lett.*, vol. 10, no. 8, pp. 1133–1135, Aug. 1998.

[4] C. van Dam *et al.*, "Novel compact polarization converters based on ultra short bends," *IEEE Photon. Technol. Lett.*, vol. 8, no. 10, pp. 1346–1348, Oct. 1996.

[5] V. P. Tzolov and M. Fontaine, "A passive polarization converter free of longitudinally-periodic structure," *Opt. Commun.*, vol. 127, pp. 7–13, Jun. 1996.

[6] J. Z. Huang, R. Scarmozzino, G. Nagy, M. J. Steel, and R. M. Osgood Jr., "Realization of a compact and single-mode optical passive polarization converter," *IEEE Photon. Technol. Lett.*, vol. 12, no. 3, pp. 317–319, Mar. 2000.

[7] Y. C. Zhu, F. H. Groen, D. H. P. Maat, X. J. M. Leijtens, and M. K. Smit, "Design of a short polarization converter on InP/InGaAsP using asymmetrical waveguides," in *Proc. Symp. IEEE/LEOS Benelux Chapter*, Delft, The Netherlands, Oct. 30, 2000, pp. 227–230.

[8] B. Jalali, S. Yegnanarayanan, T. Yoon, T. Yoshimoto, I. Rendina, and F. Coppinger, "Advances in silicon-on-insulator optoelectronics," *IEEE J. Sel. Topics Quantum Electron.*, vol. 4, no. 6, pp. 938–947, Nov./Dec. 1998.

[9] H. El-Refaei and D. Yevick, "Compact InGaAsP/InP polarization rotator," presented at the OSA Integrated Photonics Research Conf. (IPR'01), Monterey, CA, Jul. 2001, Paper ITuB5.

[10] ——, "An optimized InGaAgP/InP polarization converter employing asymmetric rib waveguides," *J. Lightw. Technol.*, vol. 21, no. 6, pp. 1544–1548, Jun. 2003.

[11] B. M. A. Rahman, S. S. A. Obayya, N. Somasiri, M. Rajarajan, K. T. V. Grattan, and H. A. El-Mikathi, "Design and characterization of compact single-section passive polarization rotator," *J. Lightw. Technol.*, vol. 19, no. 4, pp. 512–519, Apr. 2001.

[12] N. Somasiri, B. M. A. Rahman, and S. S. A. Obayya, "Fabrication tolerance study of a compact passive polarization rotator," *J. Lightw. Technol.*, vol. 20, no. 4, pp. 751–757, Apr. 2002.

[13] L. Vincetti, A. Cucinotta, S. Selleri, and M. Zoboli, "Three-dimensional finite-element beam propagation method: Assessments and developments," *J. Opt. Soc. Amer. A, Opt. Image Sci.*, vol. 17, no. 6, pp. 1124–1131, Jun. 2000.

[14] D. Correia, J. P. da Silva, and H. E. Hernandez-Figueroa, "Genetic algorithm and finite-element design of short single-section passive polarization converter," *IEEE Photon. Technol. Lett.*, vol. 15, no. 7, pp. 915–917, Jul. 2003.

[15] T. Lu and D. Yevick, "A vectorial boundary element method analysis of integrated optical waveguides," *J. Lightw. Technol.*, vol. 21, no. 8, pp. 1793–1807, Aug. 2003.

[16] D. Yevick, J. Yu, W. Bardyszewski, and M. Glasner, "Stability issues in vector electric field propagation," *IEEE Photon. Technol. Lett.*, vol. 7, no. 6, pp. 658–660, Jun. 1995.

[17] D. Yevick, "The application of complex Pade approximants to vector field propagation," *IEEE Photon. Technol. Lett.*, vol. 12, no. 12, pp. 1636–1638, Dec. 2000.

[18] M. Koshiba and Y. Tsuji, "Curvilinear hybrid edge/nodal elements with triangular shape for guided-wave problems," *J. Lightw. Technol.*, vol. 18, no. 5, pp. 737–743, May 2000.

[19] M. Koshiba, S. Maruyama, and K. Hirayama, "A vector finite element method with the high-order mixed-interpolation-type triangular element for optical waveguide problems," *J. Lightw. Technol.*, vol. 12, no. 3, pp. 495–502, Mar. 1994.

[20] M. Koshiba and K. Inoue, "Simple and efficient finite-element analysis of microwave and optical waveguides," *IEEE Trans. Microwave Theory Tech.*, vol. 40, no. 2, pp. 371–377, Feb. 1992.

[21] R. A. Soref, J. Schmidtchen, and K. Petermann, "Large single-mode rib waveguides in GeSi–Si and Si-on-SiO_2," *IEEE J. Quantum Electron.*, vol. 27, no. 8, pp. 1971–1974, Aug. 1991.

[22] O. Powell, "Single-mode condition for silicon rib waveguides," *J. Lightw. Technol.*, vol. 20, no. 10, pp. 1851–1855, Oct. 2002.

[23] S. P. Pogossian, L. Vescan, and A. Vonsovici, "The single-mode condition for semiconductor rib waveguides with large cross section," *J. Lightw. Technol.*, vol. 16, no. 10, pp. 1851–1853, Oct. 1998.

[24] A. G. Rickman, G. T. Reed, and F. Namavar, "Silicon-on-insulator optical rib waveguide loss and mode characteristics," *J. Lightw. Technol.*, vol. 12, no. 10, pp. 1771–1776, Oct. 1994.

[25] U. Fischer, T. Zinke, J.-R. Kropp, F. Arndt, and K. Petermann, "0.1 dB/cm waveguide losses in silicon-on-insulator," *IEEE Photon. Technol. Lett.*, vol. 8, no. 5, pp. 647–648, May 1996.

[26] H. Deng, D. Yevick, C. Brooks, and P. Jessop, "Design procedures for slanted-angle SOI polarization rotators," presented at the OSA/IEEE 2004 Optical Fiber Communication Conf. (OFC'04), Paper MF-41, Los Angles, CA, Feb. 22–27, 2004.

[27] C. Brooks, P. Jessop, H. Deng, and D. Yevick, "Polarization rotating waveguides in silicon on insulator," presented at the OSA 2004 Integrated Photonics Research Conf. (IPR'04), Paper IFG4, San Francisco, CA, Jun. 30–Jul. 2 2004.

Henghua Deng was born in Hunan, China, in 1976. He received the Master's degree in electrical engineering from Peking University, Beijing, China, in 2000 with a thesis focusing on employing new arrayed-waveguide grating (AWG) devices into optical add–drop multiplexers (OADMs) and improving its crosstalk and loss performances. He is currently working toward the Ph.D. degree in electrical engineering at the University of Waterloo, Waterloo, ON, Canada.

He was with the National Optical Communication Laboratory, Peking University, from 1997 to 2000, and worked on OADMs in all-optical networks for National 863 High Technology and National Natural Science Foundation (NSF) projects. His current research includes numerical methods (e.g., the finite-element method and the beam-propagation method) in integrated optics, passive optical waveguides, silicon-on-insulator-based polarization converters and AWGs.

Mr. Deng is a Member of the Optical Society of America (OSA).

David O. Yevick (SM'86–F'96) received the Ph.D. degree from Princeton University, Princeton, NJ, in 1977.

He is a Professor at the University of Waterloo, Waterloo, ON, Canada. He has written more than 120 papers involving the application of numerical and analytic procedures to optical fibers, integrated optics, and semiconductor laser modeling and is currently engaged as well in developing computational methods for optical communication system analysis.

Dr. Yevick is a Fellow of the Optical Society of America (OSA) and the American Physical Society (APS) and serves as an Associate Editor of the *Journal of the Optical Society of America A*.

Chris Brooks received the B.Sc. degree in medical physics from the Department of Physics, McMaster University, Hamilton, ON, Canada. He is currently working toward the M.A.Sc. degree from the Department of Engineering Physics at the Centre for Electrophotonic Materials and Devices (CEMD), McMaster University, focusing on fabricating and characterizing polarization rotators in silicon-on-insulator (SOI).

During his undergraduate studies, he completed co-op work terms in biomedical optics research at the Hamilton Regional Cancer Centre and in telecommunications product development at JDS Uniphase, Ottawa, ON, Canada. His research interests are in SOI-based passive waveguide devices.

Paul E. Jessop (M'95) received the B.Sc. degree in physics from the University of Waterloo, Waterloo, ON, Canada, in 1973 and the A.M. and Ph.D. degrees in physics from Harvard University, Cambridge, MA, in 1975 and 1978, respectively.

He joined the Electrical Engineering Division of the National Research Council of Canada, Ottawa, ON, Canada, in 1978, where he worked in the area of laser spectroscopy of solids. Since 1981, he has been with McMaster University, Hamilton, ON, Canada, where he is currently a Professor in the Department of Engineering Physics and Chair of the department. His principal research interests are in the areas of integrated optics and semiconductor optoelectronic devices. He heads an active research group of about eight people, consisting of both graduate students and full-time research professionals.